Estimating Blur at the Brain Gray-White Matter Boundary for FCD Detection in MRI

Xiaoxia Qu, Ljiljana Platiša, Ivana Despotović, Asli Kumcu, Tingzhu Bai,
Karel Deblaere and Wilfried Philips

Abstract— **Focal cortical dysplasia (FCD) is a frequent cause of epilepsy and can be detected using brain magnetic resonance imaging (MRI). One important MRI feature of FCD lesions is the blurring of the gray-white matter boundary (GWB), previously modelled by the gradient strength. However, in the absence of additional FCD descriptors, current gradient-based methods may yield false positives. Moreover, they do not explicitly quantify the level of blur which prevents from using them directly in the process of automated FCD detection. To improve the detection of FCD lesions displaying blur, we develop a novel algorithm called iterating local searches on neighborhood (ILSN). The novelty is that it measures the width of the blurry region rather than the gradient strength. The performance of our method is compared with the gradient magnitude method using precision and recall measures. The experimental results, tested on MRI data of 8 real FCD patients, indicate that our method has higher ability to correctly identify the FCD blurring than the gradient method.**

I. Introduction

Nowadays, approximately 50 million people are suffering from epilepsy all over the world [1], and 30% of them have focal cortical dysplasia (FCD), which is a localized malformation of brain cortical development [2]. In clinical treatments, FCD lesions are often removed by resective surgery. Before the surgery, it is essential to detect the location of FCD lesions. This is typically done using magnetic resonance imaging (MRI), which is the most important tool in the presurgical evaluation of FCD lesions [1]. However, some FCD cases still remain undetected for several reasons including the subtlety of FCD malformations, complex convolutions of the human cerebral cortex and the partial volume effect in the imaging process [2] [3].

On T1-weighted MRI scans, FCD lesions are typically characterized by [4] an increased gray matter thickness (GM-thickness, also called cortical thickness), hyper-intensity in the dysplastic lesional regions and/or the blurring of the gray-white matter boundary (GWB) which corresponds to the increased width of GWB (GWB-width). Fig. 1 illustrates the concepts of GM-thickness and GWB-width. The GM-thickness focuses on GM region while the GWB-width focuses on the transition between GM and white matter (WM). In particular, for FCD displaying blur, the voxel intensity varies slower than that within the healthy GWB as illustrated in Fig. 2. The slow-changing intensity results in the increased GWB-width.

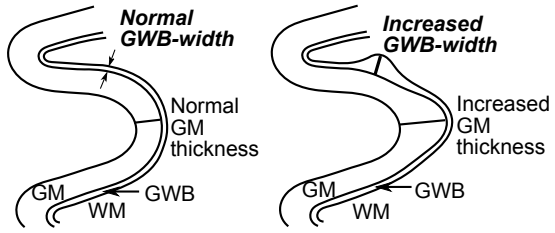

Fig. 1. An illustration of the concepts of GM-thickness and GWB-width. Regions with increased GM-thickness and/or GWB-width indicate possible FCD lesions

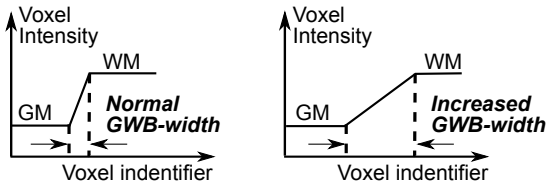

Fig. 2. Intensity change at GM/WM transition. The slower intensity transition results in the increased GWB-width (blurring of GWB) and indicates possible FCD lesions

The feature of increased GM-thickness has been exploited a lot [5] [6] [7], but the blur at GWB has been studied by few researchers [4] [8], and without a satisfactory solution. This is an important problem because some FCD lesions display only blurring of GWB (increased GWB-width) [1]. To improve the detection of this kind of FCD lesions, it is essential to estimate the GWB-width.

Previously, blurring of GWB has been detected by computing the gradient magnitude on the MRI volumes resulting in a gradient map [4]. On the gradient map, a low value of gradient magnitude represents a possible FCD lesion. However, if we look at gradient map, low gradient magnitude appears on any region with slow intensity transition (e.g. approximately flat GM and WM regions). Such regions may incorrectly be identified as FCD lesion. Therefore, the gradient magnitude method may introduce false positives (FPs). Moreover, current methods relying on the gradient magnitude do not explicitly quantify the level of blur at GWB which prevents from using them directly in the process of automated FCD detection.

This work was financially supported by the Chinese Scholarship Council and Ghent University and by the FWO project G.0.097.09.N.10.

Xiaoxia Qu is with Beijing Institute of Technology and Ghent University. Ljiljana Platiša, Ivana Despotović, Asli Kumcu and Wilfried Philips are with Department of Telecommunications and Information Processing (IPI-TELIN-iMinds), Ghent University, Ghent, Belgium. K. Deblaere is with Ghent University Hospital, Department of Radiology, Ghent, Belgium. Tingzhu Bai is with School of Optoelectronics, Beijing Institute of Technology, 100081, Beijing, China.
e-mail: Xiaoxia.Qu@telin.ugent.be

978-1-4244-7929-0/14/$26.00 ©2014 IEEE

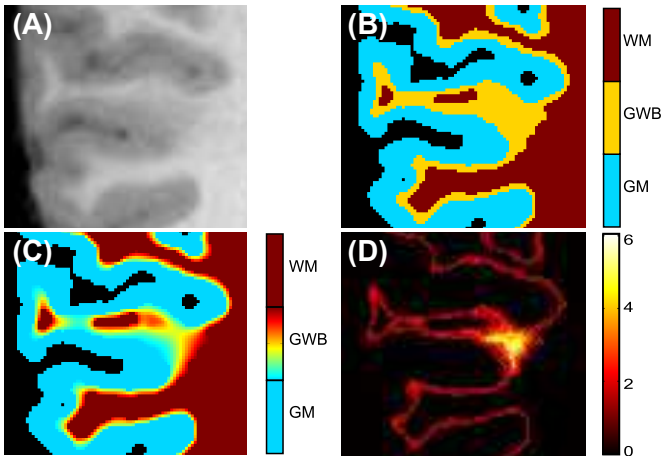

Fig. 3. Illustration of the work flow. (A) a region of the preprocessed T1-weighted MRI which includes an FCD lesion. (B) the result of brain tissue segmentation of (A) showing GM, WM and GWB regions. (C) potential map generated by modeling (B) as an electric field and solving Laplace's equation on the GWB. (D) the GWB-width calculated from (C) using our proposed ILSN algorithm; the values 0-6 denote width in mm.

To detect the FCD regions displaying blur at GWB, we propose a new method called *iterating local searches on neighborhood* (ILSN) to quantitatively measure the GWB-width. Since GWB corresponding to a FCD lesion is wider than the healthy GWB, the regions with the increased GWB-width represent possible FCD lesions.

The paper is structured as follows. In section II the test images and the proposed algorithm are explained. The results and discussion are presented in section III and finally section IV concludes this paper.

II. Methods

A. Image data and preprocessing

In this study, we selected T1-weighted MRI images of 8 patients (one image per patient) with FCD lesions, displaying blur at GWB [9]. The images were acquired at Ghent University Hospital on a Siemens 3T MRI scanner ($256\times256\times176$ voxel matrix with a resolution of 0.8594 mm $\times 0.8594$ mm $\times 0.9$ mm). In each image, a neuroradiologist (KD) manually delineated the location of the FCD lesions prior to this study. We will use this as ground truth to assess our method.

As preprocessing, we first apply automated brain extraction by Brain Extraction Tool (BET) [10] and bias correction by FSL-FAST [11]. For greater precision of our calculations, we interpolate MRI data into the resolution of 0.5 mm $\times 0.5$ mm$\times$ 0.5 mm. An example preprocessed image is shown in Fig. 3A. Note that all our computations are performed in 3D space.

B. Tissue segmentation

Our goal is to estimate the blur at GWB (increased GWB-width), so it is necessary to first extract the GWB region. To achieve this, we apply the segmentation of FSL-FAST [11] to obtain the spatial information of GM and WM, *i.e.*, the partial volume maps (PVMs) of GM and WM. The FSL-FAST segmentation is based on a hidden Markov random field model and an associated expectation-maximization algorithm. In the PVM of one tissue class (GM or WM), each voxel contains a value between 0 and 1 which represents the proportion of the class's tissue present in that voxel. As an example, a voxel in the PVM of GM with a value of 0.7 contains 70% of GM and 30% of other tissues.

Next, we use the PVMs to label the voxels of GM, WM and GWB as following,

$$L(k)=\begin{cases} L_{\mathrm{GWB}}, & 0<P_{\mathrm{GM}}(k)\cdot P_{\mathrm{WM}}(k)<1 \\ L_{\mathrm{GM}}, & P_{\mathrm{GM}}(k)=1 \\ L_{\mathrm{WM}}, & P_{\mathrm{WM}}(k)=1 \end{cases} \tag{1}$$

where $L(k)$ is the label at a given voxel k, $P_{\mathrm{GM}}(k)$ and $P_{\mathrm{WM}}(k)$ are the values in the PVMs of GM and WM, respectively. L_{GWB}, L_{GM} and L_{WM} are the labels of GWB, GM and WM volumes. An example segmented brain MRI image is shown in Fig. 3B.

C. Generating the potential map

To obtain path from GM to WM over every voxel labelled L_{GWB}, we model the GWB as an electric field [6]. In terminology of electric fields, the value at a given point is equal to the negative gradient of the electric potential at that point ψ. Here, ψ is related to the distance between the current point and the boundary of the electric field. For our application, GM and WM are taken as the boundaries of the electric field, and the potential map (Fig. 3C) is created by solving the Laplace's equation over the GWB volume.

As the initialization for solving the Laplace's equation, we take fixed values ψ_{GM}, ψ_{GWB} and ψ_{WM} as the potentials in GM, GWB and WM, respectively. To make sure there is a path from GM to WM at every voxel of GWB, these values should satisfy the following criterion: $\psi_{\mathrm{GM}}<\psi_{\mathrm{GWB}}<\psi_{\mathrm{WM}}$. For example, we take $\psi_{\mathrm{GM}}=50$, $\psi_{\mathrm{GWB}}=100$, and $\psi_{\mathrm{WM}}=150$. After solving the Laplace's equation over GWB volume, the potential values in GM and WM keep ψ_{GM} and ψ_{WM} respectively, while the potential values in GWB volume vary from ψ_{GM} to ψ_{WM} as depicted in Fig. 3C.

D. ILSN method

After producing the potential map, we estimate the GWB-width for every voxel within GWB volume. For a given voxel in GWB located at $\mathbf{b}$, let us denote by $\mathbf{g}$ and $\mathbf{w}$ the closest voxels located in GM and WM, respectively.

First, we iteratively find $\mathbf{w}$ using the following equation,

$$\mathbf{b}^{(t+1)}=\underset{\mathbf{q}^{(t)}\in N\left(\mathbf{b}^{(t)}\right)}{\arg\max}\ \psi\left(\mathbf{q}^{(t)}\right). \tag{2}$$

Here, $t\geq 1$ identifies the iteration, $\mathbf{b}^{(t)}$ is the position of the center voxel of the t-th iteration, $N(\mathbf{b}^{(t)})$ is a cubic local window ($3\times3\times3$) around $\mathbf{b}^{(t)}$, and $\mathbf{q}^{(t)}$ is the position of the neighboring voxel within $N(\mathbf{b}^{(t)})$. Iterations continue until $\psi(\mathbf{b}^{(t+1)})=\psi_{\mathrm{WM}}$, and then $\mathbf{w}=\mathbf{b}^{(t+1)}$.

Similarly, $\mathbf{g}$ can be found by iterating as follows:

$$\mathbf{b}^{(t+1)} = \underset{\mathbf{q}^{(t)} \in N\left(\mathbf{b}^{(t)}\right)}{\arg\min} \; \psi\left(\mathbf{q}^{(t)}\right). \tag{3}$$

Iterations continue until $\psi(\mathbf{b}^{(t+1)}) = \psi_{\mathrm{GM}}$, and then $\mathbf{g} = \mathbf{b}^{(t+1)}$.

Finally, we compute the GWB-width D at a given voxel (b) as

$$D\left(\mathbf{b}\right) = d\left(\mathbf{b}, \mathbf{w}\right) + d\left(\mathbf{b}, \mathbf{g}\right), \tag{4}$$

where $d(\mathbf{b}, \mathbf{w})$ is the Euclidean distance between the voxels positions $\mathbf{b}$ and $\mathbf{w}$.

After D is computed for all GWB voxels, we generate a GWB-width map for each image as illustrated in Fig. 3D. On the GWB-width map, the voxels whose width is larger than a certain threshold T ($D(\mathbf{b}) > T$) are identified as possible FCD voxels. The threshold is chosen according to the the GWB-width in healthy region.

E. Quantitative Evaluation

To evaluate the performance of our ILSN method, we compare the results to the ground truth. First, we determine the numbers of: correctly identified FCD voxels (true positives, TPs), non-FCD voxels incorrectly identified as FCD (FPs) and FCD voxels incorrectly identified non-FCD voxels (false negatives, FNs). To assess the influence of thresholds on the results, we vary the threshold T from $T_{\min}$ to $T_{\max}$ ($T_{\max} \approx 20$ mm) with a step experimentally set to 0.2 mm.

For each threshold T, we compute the *precision* and *recall*. Precision indicates how many of the positively classified voxels are relevant (true FCD) and is defined as (the number of TP)/(the number of TP + the number of FP). Recall is equivalent with sensitivity and defined as (the number of TP)/(the number of TP + the number of FN).

The values of precision and recall range from 0 to 1 and are inversely related. When precision equals 1, then all the positive results are true FCD voxels. When recall equals 1, then no FCD regions with blur at GWB are missed. Precision can be seen as a measure of exactness, whereas recall is a measure of completeness.

For comparison with an existing method, we calculate the gradient magnitude [12] on the whole MRI volumes resulting in a gradient map for each image. For fairness, we only consider in the analysis the voxels belonging to the GWB region, both for ILSN and gradient map. We vary T from $T_{\min} = 1$ to $T_{\max} = 255$ with a step of 1. Note that in the case of gradient lower values indicate more blur, thus voxels with gradient smaller than T are taken as positive results.

III. Results and Discussion

Qualitative results of the proposed and the previous method for detecting blur at GWB are shown in Fig. 4. On the gradient map, low values suggest possible FCD regions. However, it can be observed that not only FCD regions with GWB-blurring, but also GM and WM regions have low gradient values (see arrows). On the GWB-width map, the regions with large values of GWB-width correspond visually to true FCD regions in MRI images.

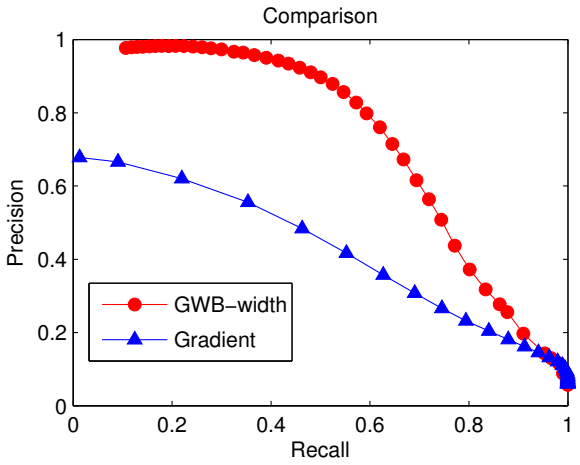

Fig. 5. Comparison of GWB-width map and gradient map with precision and recall for the MRI images of 8 real FCD patients. Every point correspondences one of the thresholds which have been mentioned on the method section. The graph shows that the GWB-width map has higher precision and recall values than the gradient map. This indicates that the GWB-width map has higher ability to correctly identify the GWB-blurring within FCD regions, and can be a good MRI feature of FCD lesions.

False positive results from GWB-width map mainly appear on the top of brain, deep gray matter, caudate nucleus and cerebellum. The presence of the FP results on the top of the brain agrees with the fact that that the blurring of GWB appears to be wider in some non-FCD regions around central sulcus (on the top of the brain) due to large amount of incoming or outgoing fibers [8]. The deep GM (two symmetrical brighter regions in Fig. 4), caudate nucleus and cerebellum regions have no clinical correlations with the FCD lesions [13]. The occurrence of FP in these FCD-irrelevant regions is mainly due to the fact that the tissue segmentation does not remove the FCD-irrelevant brain tissues. Therefore, in the future, to achieve fully automated FCD detection, those FCD-irrelevant brain tissues could be removed using a human brain MRI atlas.

The results of quantitative comparison of the two methods are presented in Fig. 5. Given the same recall, precision of the GWB-width map is larger than that of the gradient map. For example, when 50% of the FCD regions with GWB-blurring are correctly identified ($recall = 0.5$), precision is 0.91 on the GWB-width map and 0.47 on the gradient map. This indicates that using GWB-width to detect FCD blurring is more accurate than using the gradient. Given the same precision, the recall from the GWB-width map is bigger than that from the gradient map. For example, when 50% of the positive results are relevant FCD regions ($precision = 0.5$), the recall is 0.75 on the GWB-width map and 0.42 on the gradient map. This indicates that the GWB-width map has higher ability of correctly identifying the GWB-blurring within FCD regions.

The highest precision of the gradient map is 0.68, quite far from the maximum value of 1 as shown in Fig. 5. Because

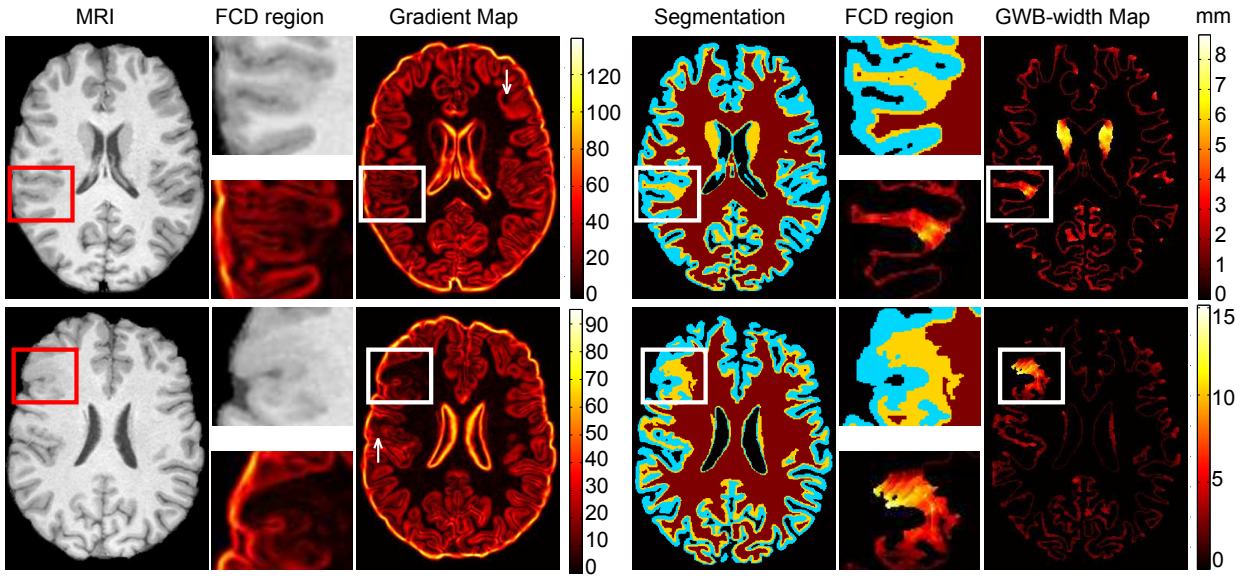

Fig. 4. The two rows correspond to two different patients. For each patient, the columns represent (from left to right): the preprocessed MR image, magnification of the squared regions from the surrounding two columns, the gradient map generated from the preprocessed MR image, the result of the tissue segmentation (colors have the same meaning as in Fig. 3B), magnification of the squared regions from the surrounding two columns, and the GWB-width map computed by the proposed ILSN method. The red and white rectangles (squared regions) denote true FCD regions (ground truth) as annotated by a neuroradiologist (KD).

the low gradient values exist not only in FCD regions with the blurring of GWB, but also on healthy GWB where there are flat intensities. On the other hand, the highest precision of GWB-width is almost 1. Because when T is large enough on GWB-width map, most of the healthy GWB volumes can be correctly recognized, so that FP is much smaller than TP producing a large precision value.

IV. Conclusion

The purpose of this study was to quantitatively analyze the blurring of GM/WM transition which is an important MRI feature for FCD detection and corresponds to increased GWB-width. Using the proposed ILSN approach, we have estimated the GWB-width and generated GWB-width maps for 8 patients with FCD lesions displaying blurring. Overall, our results demonstrate larger levels of blur (GWB-width) in FCD regions compared with the healthy regions. Moreover, the curves of precision and recall suggest that the proposed ILSN approach has higher ability of correctly identifying the FCD blurring than the gradient magnitude method. Therefore, the proposed ILSN approach for estimating the GWB-width is a good candidate for quantifying blur for FCD detection. Our future research will focus on using the GWB-width map together with other MRI features of FCD lesions and developing classifiers for fully automated FCD detection.

References

[1] A. Bernasconi, N. Bernasconi, B. C. Bernhardt, and D. Schrader, "Advances in mri for 'cryptogenic' epilepsies," *Nature reviews neurology*, vol. 7, no. 2, pp. 99–108, Feb 2011.

[2] I. Despotovic, I. Segers, L. Platisa, E. Vansteenkiste, A. Pizurica, K. Deblaere, and W. Philips, "Automatic 3d graph cuts for brain cortex segmentation in patients with focal cortical dysplasia," *Proceedings of the 33rd Annual International IEEE Engineering in Medicine and Biology Society Conference (EMBC)*, vol. 2011, pp. 7981–7984, 2011.

[3] J. Rajan, K. Kannan, C. Kesavadas, and B. Thomas, "Focal cortical dysplasia (fcd) lesion analysis with complex diffusion approach," *Comput Med Imaging Graph*, vol. 33, no. 7, pp. 553–558, Oct 2009.

[4] A. Bernasconi, S. B. Antel, D. L. Collins, N. Bernasconi, A. Olivier, F. Dubeau, G. B. Pike, F. Andermann, and D. L. Arnold, "Texture analysis and morphological processing of magnetic resonance imaging assist detection of focal cortical dysplasia in extra-temporal partial epilepsy," *Annals of Neurology*, vol. 49, no. 6, pp. 770–775, Jun 2001.

[5] R. Dahnke, R. A. Yotter, and C. Gaser, "Cortical thickness and central surface estimation," *NeuroImage*, vol. 65, no. 0, pp. 336–348, 2013.

[6] S. E. Jones, B. R. Buchbinder, and I. Aharon, "Three-dimensional mapping of cortical thickness using laplace's equation," *Human Brain Mapping*, vol. 11, no. 1, pp. 12–32, 2000.

[7] C. Hutton, E. D. Vita, J. Ashburner, R. Deichmann, and R. TurnerDei, "Voxel-based cortical thickness measurements in mri," *NeuroImage*, vol. 40, no. 4, pp. 1701 – 1710, 2008.

[8] H.-J. Huppertz, C. Grimm, S. Fauser, J. Kassubek, I. Mader, A. Hochmuth, J. Spreer, and A. Schulze-Bonhage, "Enhanced visualization of blurred gray-white matter junctions in focal cortical dysplasia by voxel-based 3d mri analysis," *Epilepsy research*, vol. 67, pp. 35–50, Oct 2005.

[9] X. Qu, A. Kumcu, L. Platisa, I. Despotovic, K. Deblaere, T. Bai, and W. Philips., "Blur estimation at the gray-white matter boundary for focal cortical dysplasia in magnetic resonance imaging," in *The 35th Annual International Conference of the IEEE Engineering in Medicine and Biology Society (EMBC) Short Papers*, no. 2961, Osaka, Japan, July 2013.

[10] S. M. Smith, "Fast robust automated brain extraction," *Human Brain Mapping*, vol. 17, no. 3, pp. 143–155, Nov 2002.

[11] Y. Zhang, M. Brady, and S. Smith, "Segmentation of brain mr images through a hidden markov random field model and the expectation-maximization algorithm," *IEEE Transactions on medical imaging*, vol. 20, no. 1, pp. 45–57, Jan 2001.

[12] S. B. Antel, A. Bernasconi, N. Bernasconi, D. L. Collins, R. E. Kearney, R. Shinghal, and D. L. Arnold, "Computational models of mri characteristics of focal cortical dysplasia improve lesion detection," *NeuroImage*, vol. 17, no. 4, pp. 1755–1760, Dec 2002.

[13] S. B. Antel, D. L. Collins, N. Bernasconi, F. Andermann, R. Shinghal, R. E. Kearney, D. L. Arnold, and A. Bernasconi, "Automated detection of focal cortical dysplasia lesions using computational models of their mri characteristics and texture analysis," *NeuroImage*, vol. 19, no. 4, pp. 1748–1759, Aug 2003.